Proceedings of the 7th International Symposium on Cavitation
CAV2009 – Paper No. 49
August 17-22, 2009, Ann Arbor, Michigan, USA

RANS simulations of a 3D sheet-vortex cavitation

Iulia Oprea
Wärtsilä
The Netherlands

Norbert Bulten
Wärtsilä
The Netherlands

ABSTRACT

On marine propellers, cavitation appearance and development is critical for performance and erosion considerations. Behind a ship, the propeller experiences all kinds of cavitation types, varying from sheet and bubbles to tip vortex cavitation.

When a cavitation analysis is required, two methods are available: experimental or numerical.

To find the optimum propeller that fits into different configurations and requirements, designers need accurate predictions within reasonable time. The experimental method is typically used at the end of a design process to verify performance. Therefore, quick and accurate numerical predictions are essential at different stages in the design process, to evaluate performance and cavitation patterns. Mathematical methods range from basic panel codes to the more complex ones, derived from the Navier-Stokes equations. Methods like DES and LES require large meshes and small time steps which makes their usability limited. The most practical viscous numerical method available at the moment in industry is Reynolds Average Navier-Stokes (RANS).

The current paper will present the results of a RANS simulation of a 2D sheet cavity and a 3D sheet-tip vortex cavitation. Accurate results of these basic simulations are steps towards the end goal, cavitating propeller simulations. In this method the viscous effects are taken into account with aid of a two equation turbulence model, which results in a reasonably fast approach due to reasonably grids requirements.

It is concluded that the RANS method can predict complex 3D sheet-vortex cavitation development and shedding. In addition, it is appropriate for industrial use because it achieves reasonably quick and accurate results. As a next step in the research project, the cavitation development on a propeller will be analyzed with this method.

INTRODUCTION

Cavitation is the vaporization of a liquid when pressure drops below the saturation pressure of the liquid. Many engineering machineries deal with appearance and disappearance of cavitation that causes noise, vibrations and erosion. The present paper deals with the interaction between sheet cavitation and vortex cavitation prediction, using numerical modeling. This interaction is an important issue for marine propeller design.

Cavitation is a design issue for all propellers. The type of cavitation can be divided in sheet, bubble and tip vortex cavitation. In this paper the emphasis will be put on the interaction of sheet-tip vortex cavitation. This type starts along the leading edge of the wing/blade and develops in to a vortex towards the tip, where a low pressure region is formed. When the pressure gets below the vapour pressure, a clear sheet-vortex cavitation can be observed in the experimental tunnel. The cavitating tip vortex is a source of noise and vibrations. For specific propeller designs, this type of cavitation is to be avoided to reduce the noise. Evaluation of the propeller design is generally based on model scale tests. However, due to costs involved in the model tests, scaling effects (see [1]) and the fact that the design process involves numerous intermediate steps to be analysed, a numerical approach is desired.

An industrial alternative for the experimental investigation of the flow around a propeller is the use of numerical methods. These methods can be split into three different groups; potential flow methods, Euler methods and Reynolds averaged Navier-Stokes (RANS) methods. A potential flow method neglects viscosity and vorticity in the flow. Since the flow phenomena in the tip region are governed by both viscosity and vorticity, it is concluded that potential flow methods are not capable of analysing complex sheet-tip vortex phenomena. Euler methods neglect viscous effects, but can take vorticity into account. This vorticity is prescribed and not affected due to the missing viscous effects. A RANS method takes both viscosity and vorticity into account. Such a method is suitable, in principle, to investigate sheet-vortex flows.

Details about the numerical approach and cavitation modelling will be discussed in the Numerical Background paragraph.

In order to quantify the CFD accuracy of a 3D cavitating flow, results of a model test are used for validation purpose. The experimental setup consists of an *Elliptic 11 Rake* hydrofoil

which is a specially designed wing to exhibit this special type of cavitation similar to a propeller. The angle of attack varies with the span, starting with 3 degrees at the tunnel walls and reaching 11 degrees at the tip. This arrangement is specially developed to produce a steady sheet cavitation at the leading edge that develops into tip vortex cavitation towards the tip of the foil. Experimental values of the forces on the foil and the velocity field are available for the cavitating flow case and can be found in [2], [3] and [4].

To validate and quantify the cavitating flow predictions of a given RANS code, simulations similar to the experiments on *Elliptic 11 Rake* are performed both in wetted and the cavitating cases. Before that, a 2D NACA profile is analyzed as a test case. For certain conditions this profile exhibits a shedding cavity, which has to be captured with the numerical cavitation model as well. In the second step, the 3D case is analyzed and the capability of a sheet-vortex cavitation prediction is investigated. Velocities and forces are compared with the experimental values for the cavitating case. Moreover, development and shedding of the sheet-tip vortex cavity are captured by the current method. The ability of unsteady RANS simulations to capture sheet-vortex cavitation development is analyzed.

Two topics of the model scale calculations will be discussed in more detail: (i) influence of the applied turbulence model and (ii) local mesh refinement in the vortex core on the cavitating results. Cavity visualization results of the *Elliptic 11 Rake* foil are compared with the pictures of experimental results of the cavity found in [4]. The validation of the numerical model is addressed and the calculated forces and velocity distributions are compared with experimental data as well. Finally, detailed results of the tip vortex cavitation formation, velocities and vorticity are analyzed.

EXPERIMENTAL SET UP

The experiments were conducted in the cavitation tunnel at Delft University of Technology. Due to the fact that the interest in the measurements and CFD is the sheet-tip vortex cavitation interaction, a special foil that gives such a cavitation pattern is investigated. Van der Hout [4] has carried out cavitating experiments on a 3D elliptic skewed hydrofoil with a finite span to investigate the interaction between sheet cavitation and vortex cavitation.

The investigated finite-span hydrofoil with tip rake and increasing angle of attack to 11 degrees at the tip is named *Elliptic 11 Rake* foil.

The focus of the experiments was to visualize the tip vortex cavitation at different angles of attack and to measure the forces to get a better understanding of the physics of the sheet and vortex cavitation interaction. Experimental results will be used and presented further when compared with the CFD results.

NUMERICAL BACKROUND

The commercial code STAR-CD version 4.02 [5] is used for all flow simulations. Flow motion equations and cavitation modeling used are presented in the current paragraph. In the present paper the numerical approach used for flow simulations are the incompressible RANS equations. In this case system of equations is formed by the mass conservation equation (1) and impulse conservation equations (2).

$$\nabla \vec{u} = 0 \qquad (1)$$

$$\rho \frac{\partial \vec{u}}{\partial t} + \rho \vec{u} \nabla \vec{u} = -\nabla p + \mu \nabla^2 \vec{u} + \rho \vec{g} \qquad (2)$$

In the conservation equations u is the velocity tensor, ρ is fluid density, g is the gravitational force tensor and μ is the viscosity of the fluid.

The turbulence models used are either the two-equation standard k-ε turbulence model or the RNG k-ε turbulence model in conjunction with the algebraic law-of-the-wall approach.

The discretization schemes are second order MARS in space and first order Euler implicit in time. The solver procedure is a steady (wetted conditions) or transient (cavitating conditions) flow calculation with SIMPLE.

Cavitation modeling available and used within the following simulations is described next. The solution methodology used can handle cavitating flows and belongs to the class of so-called interface-capturing or fixed-grid methods, also known as VOF methods. It deals with a single continuum whose properties vary in space according to its composition. The solution of the transport equations for the component fluids determines the composition.

The transport of vapor is computed according:

$$\frac{\partial \alpha_v}{\partial t} + \nabla \cdot (\alpha_v u) = S_{\alpha_v} \qquad (3)$$

In equation (3) S represents the source of volume fraction of vapor. And the volume fraction of vapor is defined as: $\alpha_v = \frac{V_v}{V}$. V_v is the fraction of the control volume V occupied by vapor.

The initial volume fraction of vapor is defined by the number of seed bubbles n_0 and their initial radius R by:

$$\alpha_v = \frac{(4/3\pi R^3) n_0}{1 + (4/3\pi R^3) n_0} \qquad (4)$$

The source term in equation (3) is defined as:

$$S_{\alpha_v} = \frac{4\pi R^2 n_0}{1 + (4/3\pi R^3) n_0} \frac{dR}{dt} \qquad (5)$$

In equation (5) the rate of change of a bubble radius is estimated using a simplified Rayleigh-Plesset equation:

$$\frac{dR}{dt} = sign(p_v - p)\sqrt{\frac{2|p_v - p|}{3\rho_L}} \qquad (6)$$

where p_v is the saturation pressure, p the local pressure around the bubble and ρ_L the density of the fluid.

The volume fraction of the components is determined from the condition:

$$\alpha + \alpha_v = 1 \qquad (7)$$

And the properties of the effective fluid vary in space according to the volume fraction of each component. Density is defined by:

$$\rho = \alpha\rho + \alpha_v\rho_v \qquad (8)$$

and viscosity:

$$\mu = \alpha\mu + \alpha_v\mu_v \qquad (9)$$

All the transport equations are the same for the effective fluid as in the single phase flow case, with the exception that density and viscosity vary sharply across the cavity surface.

NUMERICAL RESULTS

2D TEST CASE: NACA0015

Numerical modeling of cavitating flows is difficult, due to the coexistence of two fluids, water and vapor. The main issues are the treatment of the surface between the two phases and the mass transfer from one phase to another. Therefore a simple 2D test case is used as a first step for cavitation assessment.

The cavitation model described previously is analyzed in terms of grid resolution and turbulence modeling.

A NACA 0015 profile is used for wetted and cavitating flow simulations, being a benchmark test case for many researchers and therefore results for comparison purpose are available for this 2D case.

The analyzed NACA 0015 profile has an angle of attack of 6 degrees and a chord of 200 mm. The domain size is 1400 x 570 mm, therefore 2 chords at the inlet and 4 at the outlet. Profile mesh is a multi-block structured grid, with an O-grid type around the profile (including a small round trailing edge) for a good control over the y+ values, see figure 1.

Applied boundary conditions are an inlet boundary type with inlet velocity of 6 m/s and turbulence intensity of 1%, pressure boundary of 0 Pa at the outlet and slip walls at the outer domain sides.

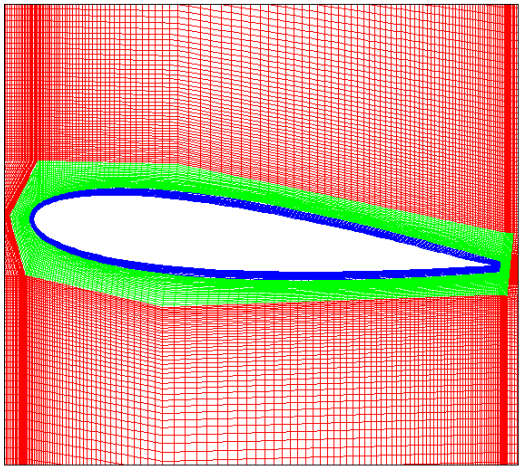

Figure 1: NACA 0015 Profile mesh

Three flow conditions are analyzed: (1) wetted flow, (2) steady cavitating flow at σ=1.6 and (3) shedding cavitating case at σ=1.0. In computation values for the water density of 998 kg/m^3 and vapor density of 0.023 kg/m^3 are used.

1. *Wetted flow case.* In this case RANS wetted flow simulations are performed over the NACA 0015 profile with the previous described settings. Results obtained for pressure coefficient and lift and drag coefficients are presented in the following for grid resolutions and turbulence modeling influence assessment.

Wetted flow pressure coefficient results, for grid G1 (250 profile vertices) and grid G2 (418 profile vertices) with the standard k-ε turbulence model and grid G2 with the RNG k-ε model are shown in figure 2.

The pressure coefficient Cp is defined by:

$$C_p = \frac{p_{relative}}{0.5\rho u^2} \qquad (10)$$

The Cp distribution along the chord for the mesh and turbulence variation is presented in figure 2.

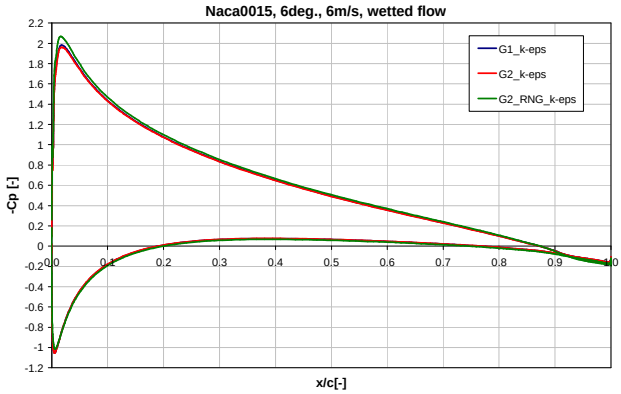

Figure 2: Pressure Coefficient NACA0015, wetted flow

Figure 2 shows little difference for all three investigated arrangements. Only near the leading edge differences can be seen at pressure and suction side. At the stagnation point the Cp

is 1.053 for grid G1, 1.054 for grid G2 and 1.016 for grid G2 with the RNG turbulence model. Over-prediction of the pressure coefficient in the stagnation point is a well known issue of the turbulence modeling; see Bulten & Oprea [1] and Moore & Moore [7]. Therefore, the best estimation in figure 2 is obtained with the grid G2 with RNG model due to the fact that is the closest to exact value of the Cp in the stagnation point, which is unity.

Non-dimensional lift and drag coefficient are defined in the by the equations (11).

$$C_L = \frac{Lift}{0.5\rho u^2 cS} \qquad C_D = \frac{Drag}{0.5\rho u^2 cS} \qquad (11)$$

Lift and drag coefficients variation with mesh and turbulence are presented in table 1.

Name	G1 k-ε	G2 k-ε	G2 RNG
Cl	0.644	0.638	0.667
Cd	0.019	0.020	0.014

Table 1: Lift and Drag Coefficients for NACA0015 profile for wetted flow condition

Lift coefficient predictions are in the same range for all analyzed cases, while drag coefficient predicted with the RNG model is lower than the predictions made with the standard k-ε. Over-prediction of the pressure in the stagnation point will result in an over-prediction of the pressure drag of a profile (see [1]). Due to the fact that stagnation pressure is better predicted with the RNG model, the corresponding drag is consequently lower. Lift coefficient is less affected by the over-prediction of the stagnation point pressure.

2. *Steady cavitating case.* In this case the cavitation model is enabled and time dependent RANS simulations are performed over NACA 0015 profile.

Using the Bernoulli equation, the cavitation number is defined as:

$$\sigma = \frac{p_0 - p_v}{0.5\rho u^2} \qquad (12)$$

From equation (10) and (12) the relation between pressure coefficient and cavitation number is defined by equation:

$$\sigma = -C_{p\min} \qquad (13)$$

The steady cavitating case results at σ=1.6 are presented and analyzed next for the same 3 cases as for the wetted flow by means of pressure and lift and drag coefficients.

The pressure coefficients for grid and turbulence model variation are shown in figure 3.

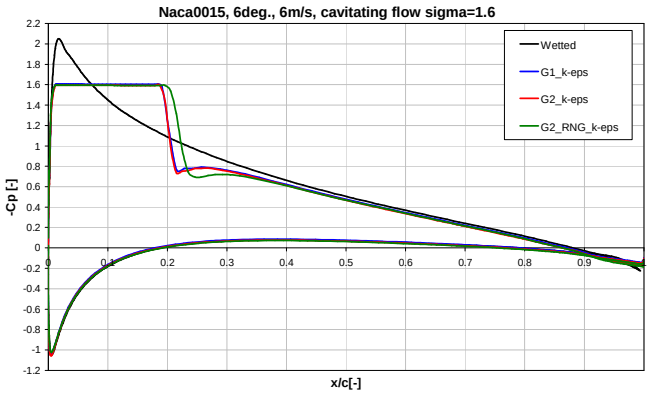

Figure 3: Pressure Coefficient NACA0015, steady cavitating flow

The figure shows a constant Cp of -1.6 in the cavitating cases. This corresponds to the leading edge cavity sheet presence and confirms that the cavitation appears when the vapor pressure is reached, see equation (13). In this case the mesh resolution and turbulence model influence is limited. The RNG model predicts a slightly longer steady cavity.

Lift and drag coefficients corresponding to the steady cavitating case are presented in table 2.

Name	G1	G2	G2 RNG
Cl	0.630	0.629	0.642
Cd	0.022	0.022	0.019

Table 2: Lift and Drag Coefficients for NACA0015 profile for steady cavitating flow condition

From tables 1 and 2 the influence of the cavitation over the profile performance is assessed. Lift coefficient is decreasing and drag coefficient is increasing compared with the wetted flow case, when cavitation is present. Grid and turbulence variation have limited influence over lift and drag prediction results in this case, like in the wetted flow case.

3. *Shedding cavitating case.* The third case in this 2D study is represented by a time dependent shedding cavitating flow case at σ=1.0. A lower cavitation number implies more cavitating fluid and appearance of instabilities and shedding of cavity clouds.

When analyzing the unsteady cavitating case at σ=1.0 the differences between the turbulence models used are noticed. The mesh refinement, time steps and inlet values for turbulence have no influence on results using the standard k-ε model. The cavity is slowly increasing and decreasing periodic in time without shedding. When the RNG model is used the cavity becomes highly unsteady and the cavity starts shedding. In figure 6 the cavity volume variation in time for grid resolution and turbulence modeling influence is shown.

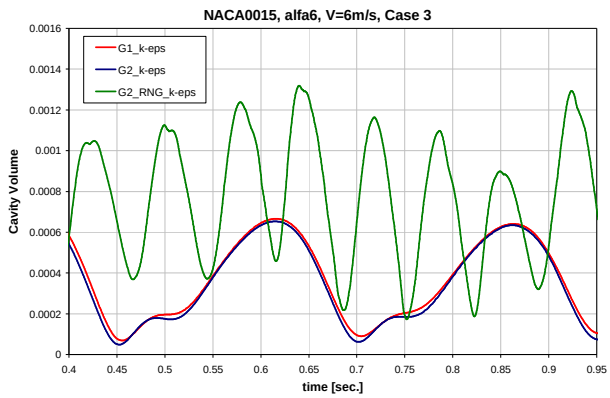

Figure 4: Cavity volume variation in time

The RNG model produces less turbulent viscosity at the water-vapor interface, leading to a strong reentrant jet which is capable of detaching the tail of the cavities. Therefore, more unstable and faster shedding of the cavities can be seen in figure 4.

Figure 4 shows that the cavity oscillations are insensitive to different grid resolution with the standard k-ε model (dark blue and red lines). When the RNG model is used for the same grid, highly unsteady and faster periodic variations in the cavity volume appear (green line). The RNG turbulence model predicts a time period of 0.07s resulting in a frequency of 14Hz, contrary to 4Hz as obtained with the standard k-ε model. In the literature for NACA 0015 frequencies from 11 to 24 are reported, see [8].

The corresponding lift coefficient variations for the unsteady cavitating case are presented in figure 5.

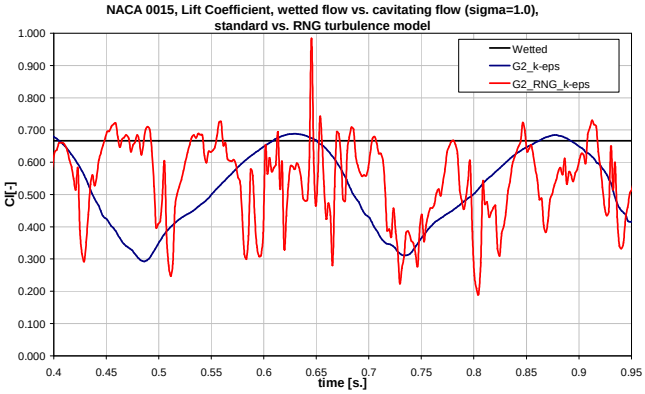

Figure 5: Lift coefficient variation in time

The lift coefficient is varying with the cavitation formation, detaching and shedding. A frequency analysis of the shedding simulation case lift and drag coefficients results in a first order frequency of 14Hz and a second order frequency of 27Hz. These high frequencies obtained for lift and drag coefficients are related to the collapse of shedding vapor structures.

This simple 2D case proves that the current method is capable of capturing complex cavitating flows: attached sheet cavity, unsteady shedding cavity, reentrant jets and vortices, when the RNG turbulence model is used. Therefore, the RNG turbulence model performs better in cavitating flows predictions and it will be used on the 3D case simulations.

3D CASE: ELLIPIC 11 RAKE WING

The geometry used for three-dimensional case is an *Elliptic 11 Rake* wing, with a NACA0009 profile, root chord of 0.15 m and tip chord 0.05m as described in [4].

The numerical domain sizes are: inlet location at 2 root chords upstream of leading edge, outlet at 3 root chords downstream of trailing edge and a normal test section of 2 by 2 root chords, as in the experimental setup, see figure 6.

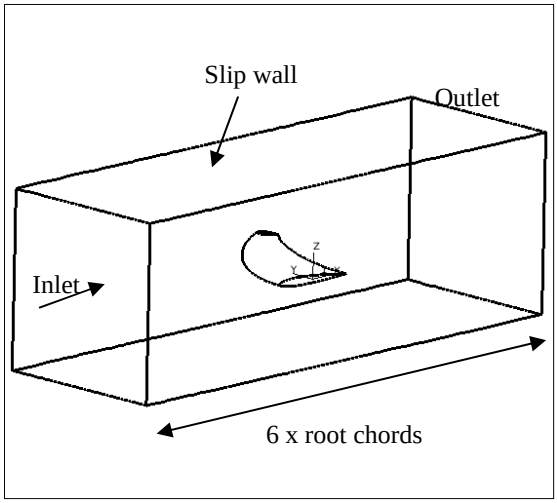

Figure 6: Computational domain of Elliptic 11 rake hydrofoil

The mesh for the wing is created with a structured multi-block hexagonal mesh generator. The mesh near the blades is based on a C-grid type (sharp trailing edge), to maintain control over the quality of the mesh near the blade. Development of the boundary layer along the blade surface is taken into account using wall functions. The requirements for the y+ values on the foil surface can be met with an acceptable number of cells in the normal direction. Moreover, the aspect ratio and the differences in cell sizes can be kept low. Figure 7 shows the surface mesh of the *Elliptic 11 Rake* hydrofoil.

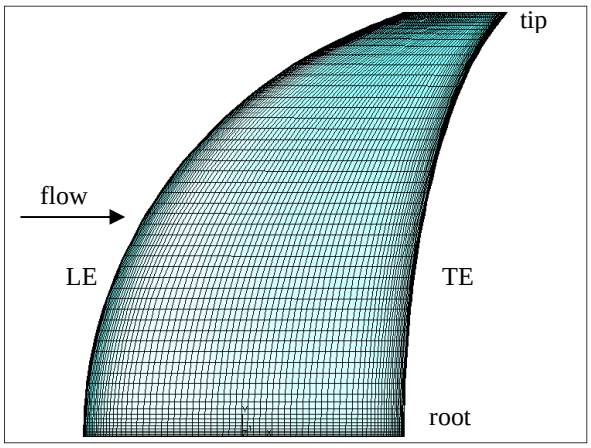

Figure 7: Surface mesh of Elliptic 11 Rake hydrofoil

The C-grid around the profile is shown in figure 8. This type of meshing is efficient for y+ control, which is kept constant for all grid variations, with values between 15 and 100, as recommended for the wall function approach [5].

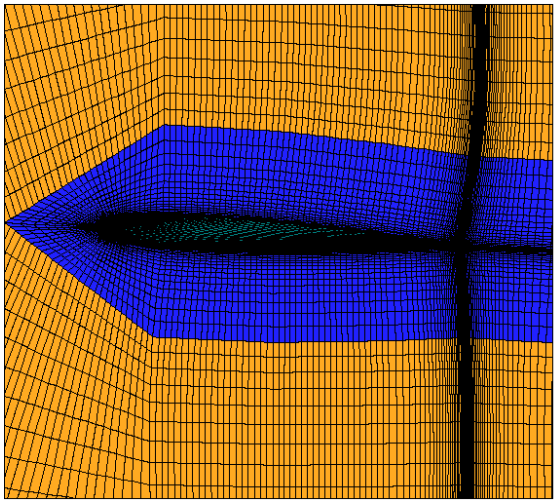

Figure 8: Cross-sectional mesh of Elliptic 11 rake hydrofoil

Applied boundary conditions are at the upstream an inlet boundary condition, which requires the prescription of the velocity components and additional values for the turbulence. At the outlet boundary downstream, a constant pressure boundary condition is applied. This condition enables both inflow and outflow at the outer surface. At the domain sides slip wall boundaries are applied. Figure 6 shows the computational domain and the location of the boundary conditions.

The reference Cartesian coordinate system has the X axis on chord-wise flow direction, Y axis in span-wise direction and Z axis is normal to the inflow.

A detailed numerical investigation is made on the *Elliptic 11 Rake* geometry in wetted flow case and cavitating case, with different grid resolutions and angles of attack. Also, based on the available data, predicted forces and velocities are compared with the experiment results.

WETTED FLOW RESULTS

The *Elliptic 11 Rake* foil is first computed in a wetted flow condition for an inlet velocity of 7.43 m/s and an outlet pressure value of 21700 Pa. Grid influence is assessed from four generated meshes, see table 1. Grids G2 and G3 are build based on an over-all mesh refinement of the grid G1 with a grid ratio of $\sqrt{2}$. Then from grid G3 a fourth mesh is created based on the cells that correspond to the tip vortex location, determined with the Q-factor criterion (see equation (14)) and refined in all X, Y, Z directions with 2 by 2 by 2.

Cells	G1	G2	G3	G3_ref
Fluid	287392	569200	1180928	1851892
Profile	96	136	192	192

Table 3: Grid cells number for different meshes

From grid G1 to G3 the over all mesh refinement influence is analyzed, while from grid G3 to G3_ref the effect of the locally mesh refinement at tip vortex location is evaluated.

The non-dimensional lift and drag coefficient are defined as in the equations (11) and their variation with grid resolution quantified in table 4.

Name	G1	G2	G3	G3_ref
Cl	0.1279	0.1268	0.1266	0.1274
Cd	0.00981	0.00901	0.00899	0.00898

Table 4: Lift and drag coefficients for different meshes for wetted flow condition

Refining the overall mesh (grids G1, G2 and G3) decreases lift and drag coefficients. Local vortex refinement has limited effect on drag and slightly increases lift.

Variation of lift and drag with angle of attack β are also investigated and there results are shown figure 9. Lift increases linear with β, while drag increases parabolic with β. The variation of the lift and drag with the angle of attack is agreement with experience, see [9].

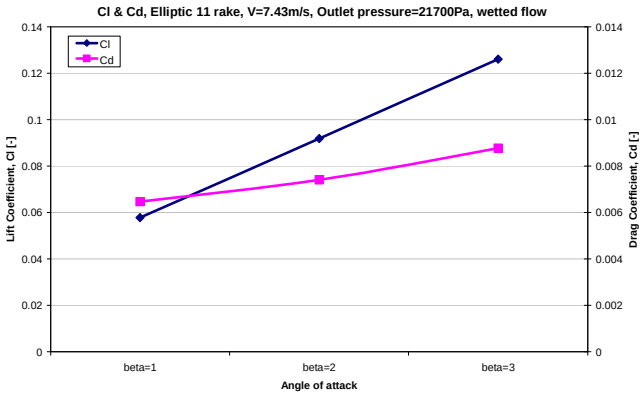

Figure 9: Cl and Cd variation with angle of attack, wetted flow

TIP VORTEX FLOW

The main interest of the current investigation is the tip vortex flow region. To asses the grid resolution influences over the tip vortex simulations, pressure, velocity and vorticity (Q-factor) are analysed, downstream of the foil at x=0.15m (see figure 10) through the vortex core.

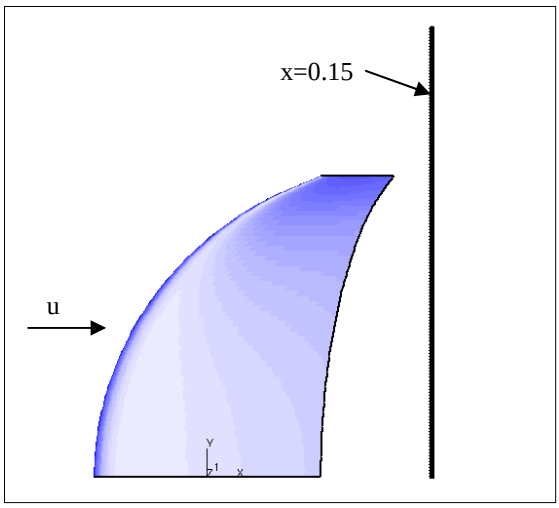

Figure 10: Plane x=0.15 location, downstream of the foil

When dealing with vortex topics like vortex definition, detection and visualization are important to be addressed. Along the years many vortex definitions have been attempted, but not with much success. Its definition remains vague and therefore its predictions and detection arguable. One of the first and most general definitions is made by Lugt and states that "a vortex is the rotation motion of a multitude of material particles around a common centre" see [10]. Due to this uncertainty there are numerous vortex detection methods more or less successful but not a definitive one. Still, one of the most successful methods are the Galilean invariant methods, and the Q-criterion being one of the most simplest in definition and implementation among the other two, $\lambda 2$ and Δ, see [11].

The Q factor criterion is implemented in the CFD and used in the present paper to capture high swirling flow regions/vortices. The Q factor is defined by:

$$Q = \frac{1}{2}\left[\left(\frac{\partial u_i}{\partial x_i}\right)^2 - \frac{\partial u_i}{\partial x_j}\frac{\partial u_j}{\partial x_i}\right] \qquad (14)$$

When Q>0 the rotation is dominant and the region determines a vortex tube. Note that the local vortex refinement is made using cells with high Q-factor values, higher than a certain positive values chosen by the user.

The vortex core pressure coefficient values are influenced by the grid resolution as shown in figure 11.

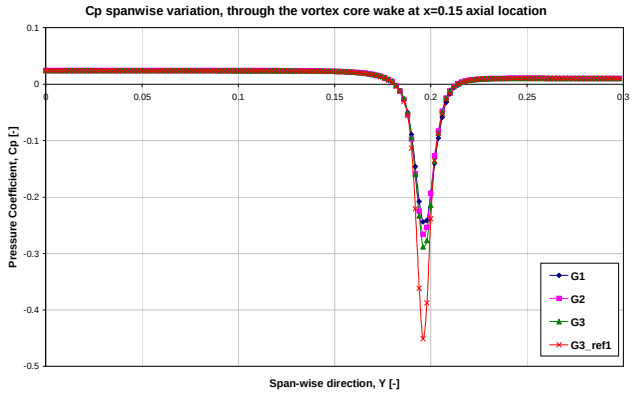

Figure 11: Cp variation with mesh, wetted flow

For increasing mesh density, the minimum pressure within the vortex core is decreasing. Overall mesh refinement (grids G1, G2 and G3) improves the Cp prediction but a locally refined mesh (G3_ref) gives the most important step in the prediction of the low pressure within the tip vortex core.

Accurate predictions of velocity components at tip vortex location are important to determine the vortex location by means of the Q-factor criterion. Influence of the mesh resolution over axial and normal velocity components are presented is figures in 12 and 13.

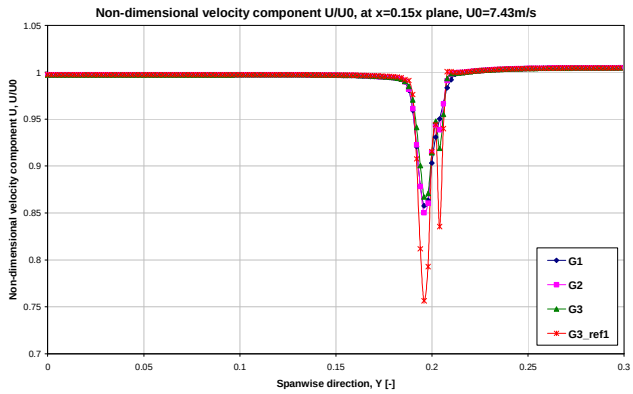

Figure 12: Non-dimensional velocity U in flow direction for 4 meshes

The U-component velocity (in flow direction) through the vortex core is lower than in the rest of the field. Higher mesh resolution is decreasing further the minimum value within the vortex core. The local mesh refinement gives the highest improvement.

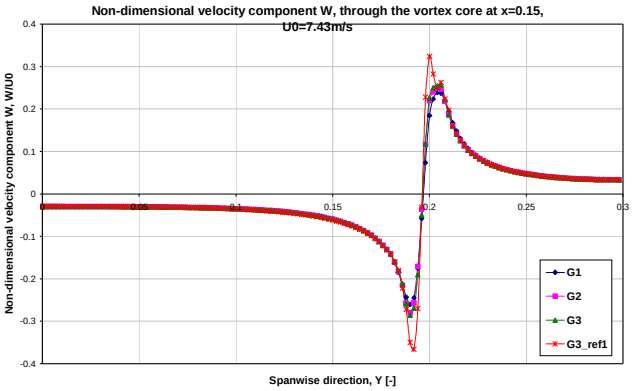

Figure 13: Non-dimensional velocity W in normal direction for 4 mesh variants

The minimum and maximum values of the velocity component normal to the flow are improved when local mesh refinement is applied, as shown in figure 13.

The Q-factor prediction is also influenced by mesh density as presented in figure 14.

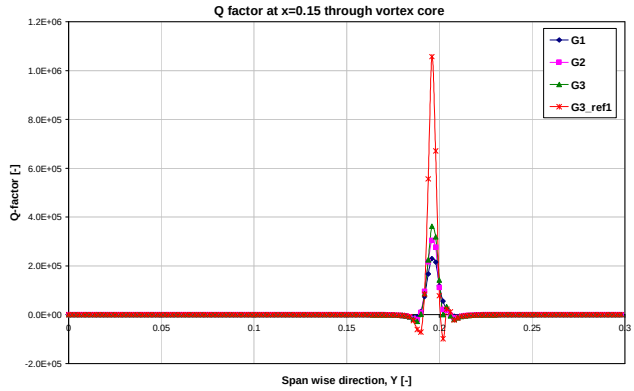

Figure 14: Q-factor for 4 mesh variants

From equation (14) it is known that a vortex is defined as a flow region where the Q is positive. Therefore in figure 14 the high peaks of the Q-factor values downstream of the foil indicate a vortex region, as seen also in pressure coefficient and velocity components. Local vortex refinement applied to grid G3 is very important, obtaining a Q-factor value of 106000 for G3_ref instead of 36000 for the grid G3. Therefore the vortex is better predicted with a fine mesh. Still downstream of the analysed plane (x=0.15), the vortex is fast decaying in strength. Further refinement may be needed to capture the accurate behaviour of strong downstream vortices.

When dealing with tip vortices local refinement is crucial for accurate predictions of pressure and velocity components with its core.

CAVITATING FLOW RESULTS, σ=0.68

When cavitation is present on the *Elliptic 11 Rake* foil, lift and drag coefficients, pressure coefficients and velocities are influenced as presented in this section. Results of the RANS cavitation simulation are shown and validated with the available experimental results.

The influence of cavitation over the foil on lift and drag coefficients is shown in table 5, where the first column is the wetted flow, second column is the cavitating flow and third the experimental cavitating result.

Name	CFD Wetted	CFD σ=0.68	EXP σ=0.68
Cl	0.1274	0.1311	0.1297
Cd	0.00898	0.01166	0.00935

Table 5: Lift and drag coefficients for wetted flow and cavitating flow compared to experimental data

Compared with the wetted flow case the lift and drag are increasing when cavitation is enabled. Cavitating results are close to the experimental ones for lift and slightly higher for drag.

The pressure coefficient for the wetted flow and the cavitating flow is presented in figure 15.

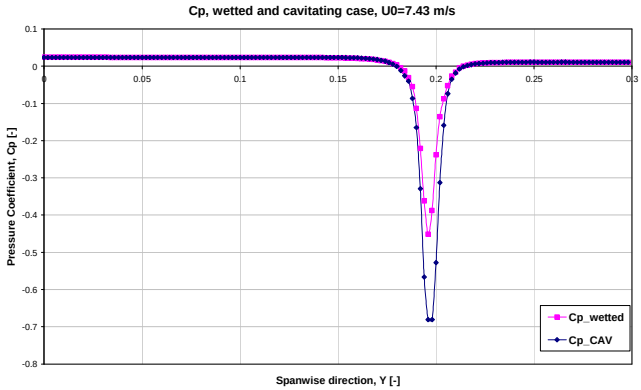

Figure 15: Cavitation influence over Cp

From figure 15 can be seen that the pressure coefficient is decreasing due to the cavitation modelling within the vortex core. The minimum pressure coefficient is -0.68 in agreement with the analysed cavitation number, see equation (13).

The velocity in flow direction through the vortex core is decreasing when cavitation is enabled as shown in figure 16. Within the highly swirling region of the vortex, the axial velocity is decreasing, while the normal components are increasing. This is enhanced when cavitation is present, as shown in figures 16 and 17.

The differences found in pressure distribution and velocity components can be explained by a reduction of the viscosity in the cavitating vortex core, according to equation (9).

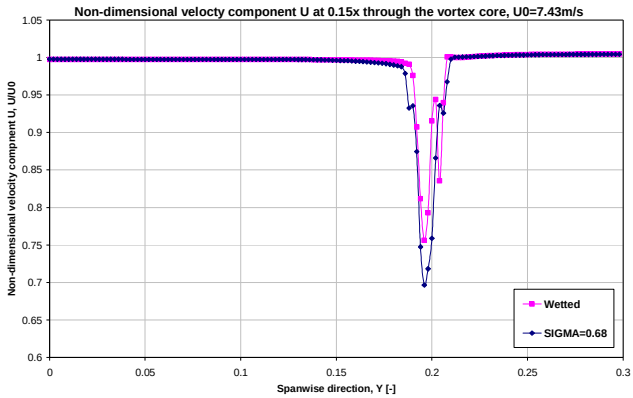

Figure 16: Non-dimensional velocity component U in flow direction for wetted and cavitating flow

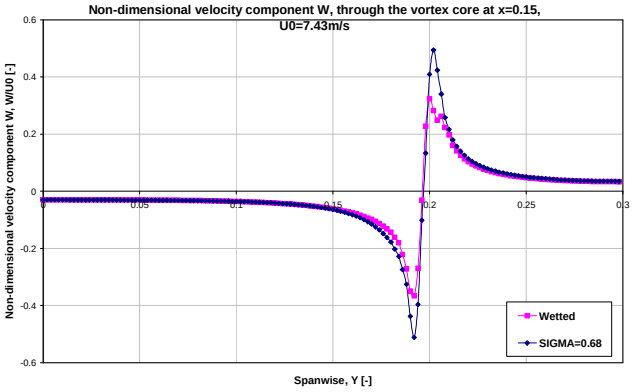

Figure 17: Non-dimensional velocity component W in normal direction for wetted and cavitating flow

Tip vortex cavitation is decaying fast downstream of the x=0.15 plane. For strong cavitating vortices downstream, very fine local meshes are required.

TIP VORTEX CAVITATION VISUALIZATION

Experimental visualization results for the *Elliptic 11 Rake* foil are available in [3]. In figure 18 the case with angle of attack β=3, velocity inlet 7.43 m/s, σ=0.68 is shown.

The current RANS simulations for the same condition as in the experiments in figure 18 are show for comparison and validation purpose in figure 19.

Figures 18 and 19 show the visualization of the cavity based on experiments and on computations. For a volume fraction iso-surface of 1%, the simulated cavity shape and volume are comparable with the experimental ones. Also the starting point of the re-entrant jet (1) and of the tip vortex formation and detachment (2), see figure 19, is very well in agreement with the experimental observations, see figure 18. Changes in the volume fraction iso-surface, have limited influence on cavity shape visualization, only small variations of the volume can be noticed.

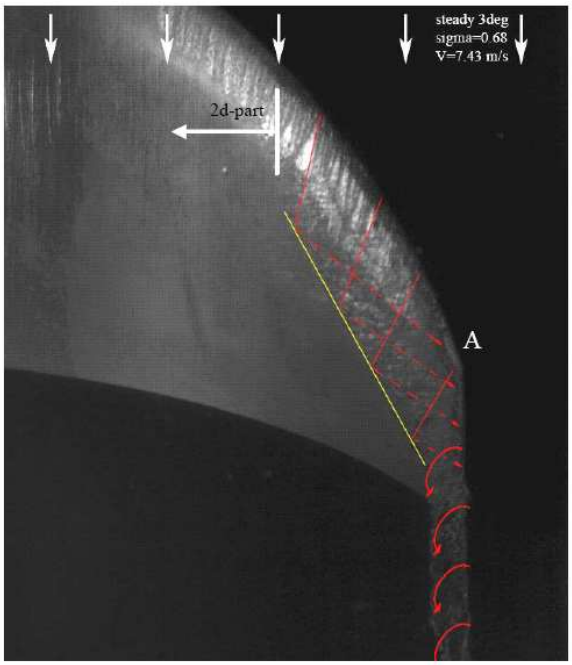

Figure 18: Experiments cavitation visualization at σ=0.68, β=3, u=7.43 m/s, taken from [3]

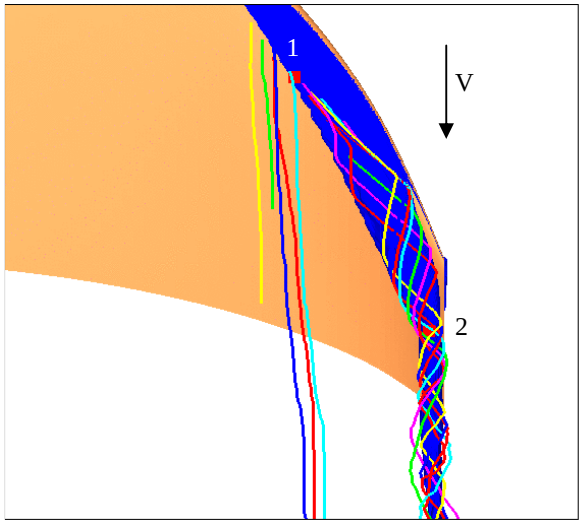

Figure 19: RANS simulations, particle tracks and cavitation volume fraction iso-surface=0.007, at σ=0.68, β=3, u=7.43 m/s

CONCLUSIONS

The scope of the present paper is to give an approach to successful predictions of the complex cavitation phenomena using a CFD method for industrial use.

At the end of the current study, two main conclusions should be outlined.

- First, the k-ε RNG turbulence model proves to be the most important ingredient in successful shedding cavitation simulations for two-dimensional NACA

0015 profile with good results for the cavitation shedding pattern and frequencies.

- Second, with an appropriate mesh, focused on the sheet-tip vortex cavitation region, the exhibited tip vortex is well captured. Results of the simulations for the foil forces, velocities and cavitation pattern are in agreement with the measurements and experimental observations for a complex 3D *Elliptic 11 Rake* foil.

Thus, the k-ε RNG turbulence model in combination with a local refined mesh of the tip vortex region proves to be a good recipe for successful simulations of cavitation prediction when using CFD approach.

In a next step all the knowledge acquired within the present research is going to be applied on propellers for sheet-tip vortex cavitation assessment.

NOMENCLATURE

c	Chord length	[m]
Cd	Drag coefficient	[-]
Cl	Lift coefficient	[-]
Cp	Pressure coefficient	[-]
Cr	Chord length at the root	[m]
Ct	Chord length at the tip	[m]
n_0	Number of seed bubbles	[-]
p	Pressure	[Pa]
p_v	Vapour pressure	[Pa]
R	Bubble radius	[m]
S	Span	[m]
$S_{\alpha v}$	Source of volume fraction of vapor	[1/s]
T	Time	[s]
Q	Second invariant of the velocity gradient tensor	[$1/s^2$]
U	Velocity component in X direction	[m/s]
V	Volume	[m^3]
V_v	Fraction of control volume V	[-]
W	Velocity component in Z direction	[m/s]
X, Y, Z	Flow field coordinate system	[-]
X	Flow direction	[-]
Y	Span-wise direction	[-]
Z	Normal direction	[-]
α	Volume fraction	[-]
α_v	Volume fraction of vapor	[-]
β	Angle of attack	[deg]
μ	Viscosity	[Pa·s]
ρ	Density	[kg/m^3]
σ	Cavitation number	[-]

REFERENCES

[1] Bulten N. and Oprea A.I., Consideration on deviations in torque prediction for propellers and waterjets with RANS codes, RINA 2005, Southampton, UK

[2] Foeth E. J. 2008, The structure of Three-Dimensional Sheet Cavitation, PhD thesis, Delft University of Technology.

[3] Foeth E. J. and van Terwisga T. 2006, An attached cavity on a three-dimensional hydrofoil, CAV2006, Wageningen, The Netherlands.

[4] A.J. van der Hout. 2007, The interaction of sheet and vortex cavitation, Master's thesis, Technical University of Delft, The Netherlands.

[5] STAR-CD Version 4.02 Methodology, CD-adapco Group, 2006

[6] Bulten N. and Oprea A.I., Evaluation of McCormick's rule for propellers tip cavitation based on CFD results, CAV 2006, Wageningen, The Netherlands

[7] Moore, J.G., Moore, J., 1997, Controlling over-production of turbulence in two-equation models by limiting the anisotropy of the Reynolds normal stresses, 1997 ASME Fluids Engineering Division summer meeting.

[8] Koop A., 2008, Numerical Simulation of Unsteady Three-Dimensional Sheet Cavitation, PhD thesis, University of Twente, Enschede, The Netherlands.

[9] Abbot I. and Doenhoff A., Theory of wing sections, 1959

[10] Banks D.C. and Singer B.A., 1994, Vortex Tubes in Turbulent Flows: Identification, representation, reconstruction Proceedings of IEEE Visualization '94

[11] Sahner J., Weinkauf T., Hege H.-C., Galilean invariant extraction and iconic representation of vortex core lines, Eurographics / IEEE VGTC Symposium on Visualization, UK, 2005